X-ray diffraction and QTAIM calculations of the non-covalent intermolecular fluorine-fluorine interactions in tris(trifluoroacetylacetonato)-manganese(III)

Roxanne Gostynski [a] *Petrus H.van Rooyen,* [b] *Jeanet Conradie* [a,c] *

[a] Department of Chemistry, PO Box 339, University of the Free State, 9300 Bloemfontein, Republic of South Africa.

[b] Department of Chemistry, University of Pretoria, Private Bag X20, Hatfield, 0028, South Africa.

[c] Department of Chemistry, University of Tromsø, N-9037 Tromsø, Norway

*Contact author details:

Name: Jeanet Conradie

Tel: +27-51-4012194; Fax: +27-51-4017295

e-mail: conradj@ufs.ac.za

TOC:

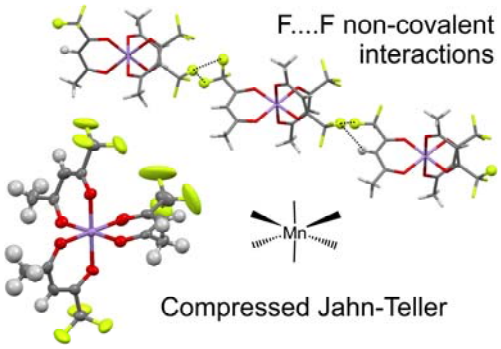

Synopsis:

X-ray structure of tris(trifluoroacetylacetonato)-manganese(III) shows compression Jahn–Teller distortion and F...H and F...F non-covalent intermolecular interactions.

Highlights

- Structure of tris(trifluoroacetylacetonato)-manganese(III), [Mn(tfaa)$_3$]
- Structure of [Mn(tfaa)$_3$] exhibit compression Jahn–Teller distortion
- Crystal of [Mn(tfaa)$_3$] shows intermolecular F-F non-covalent interactions
- QTAIM of [Mn(tfaa)$_3$] pairs shows intermolecular F-F bond paths

Keywords:

Mn(III); β-diketone; DFT; structure; F···F non-covalent interactions; Jahn–Teller distortion

Abstract

An X-ray study was conducted on tris(trifluoroacetylacetonato)-manganese(III). The two different molecules in the unit cell exhibit a distorted octahedral geometry and moderate compression Jahn–Teller distortion respectively. A number of F...H and F...F intermolecular interactions were observed in the packing of the crystals in the solid state. The crystal packing effects could lead to the observed compressed Jahn–Teller distortion, instead of the expected elongation Jahn–Teller distortion. A Quantum Theory of Atoms in Molecules (QTAIM) study on selected molecular pairs identified intermolecular bond paths (BP) between fluorine atoms with bond critical points (BCP) which have positive electron density (ρ) and Laplacian of electron density ($\nabla^2\rho$) values, which are indicative of weak F···F non-covalent bonding interactions.

1 Introduction

Tris(β-diketonate)-manganese(III) complexes, [Mn(β-diketonato)$_3$], have various applications as homogeneous [1,2,3,4,5,6] and heterogeneous [7] catalysts. Recently, the stability of [Mn(β-diketonato)$_3$] complexes as redox mediators in dye-sensitized solar cells (DSSCs) was investigated. It was found that "although the results obtained with tris(β-diketonate)Mn complexes have still been unsatisfactory with respect to other alternative metal based redox mediators, it can be foreseen that the use of sterically hindered dyes, compatible with an appropriate photoanode passivation and TiO_2 optimization, may lead to better DSSC performances, which will also allow a deeper understanding of the charge transfer dynamics involving this new class of redox relays" [8]. A fundamental knowledge of all the properties, including non-covalent intermolecular interactions that can influence the solid state structure of these complexes, contributes to the understanding of the chemical behaviour of [Mn(β-diketonato)$_3$].

High spin [Mn(β-diketonato)$_3$] complexes with four unpaired electrons [9,10] result in a ^5E_g ground state in an octahedral environment, which is susceptible to Jahn–Teller distortions. The filling of the four d electrons can be either $(t_2g)^3(d_{z2})^1(d_{x2-y2})^0$ or $(t_2g)^3(d_{z2})^0(d_{x2-y2})^1$, leading to tetragonal elongation (TE) and compression (TC) Jahn–Teller distortion respectively. The different experimental solid state structures of [Mn(acac)$_3$] (Hacac = acetylacetone) are described as five different forms, namely the α, β, γ, δ and ε forms [11]. Reported structures of [Mn(β-diketonato)$_3$] include structures with Jahn–Teller tetragonal compression (TC, the β form) [4,12,13], Jahn–Teller tetragonal elongation (TE, the γ form) [9,14,15], orthorhombic distortion (OD) [11] and distorted octahedron (DO) [8]. Results obtained by high-frequency and high-field electron paramagnetic resonance (HFEPR) spectroscopy on [Mn(acac)$_3$], in frozen solution free of crystal packing effects, showed that axial elongation is the "natural" form of Jahn–Teller distortion for [Mn(acac)$_3$] and that crystal packing effects could lead to compressed Jahn–Teller distortion [16] or other structures for [Mn(β-diketonato)$_3$] complexes. A mass-spectrometry controlled gas-phase electron diffraction (GED) based structure investigation on evaporated samples of [Mn(acac)$_3$] showed that [Mn(acac)$_3$] exhibits C_2 symmetry, with the central structural motif of a tetragonal elongated MnO_6 octahedron [17]. Thus, in the gas phase, free from intermolecular-interaction, the [Mn(acac)$_3$] exhibits a Jahn–Teller elongation structure. Quantum chemical calculations on the structure and spin states of [Mn(acac)$_3$] [18] and [Mn(β-diketonato)$_3$] complexes [19,20], also showed that [Mn(acac)$_3$] is high-spin with S=2, and that the ^{5}B electronic state with elongation Jahn-Teller is *c.a.* 1 kcal/mol (0.04 eV) lower in energy than the ^{5}A with compression Jahn-Teller distortion. However, intermolecular interaction in experimental solid state crystals can affect the distortion of the coordination polyhedron, leading to a higher energy electronic state. In this contribution, the solid state structure of a [Mn(β-diketonato)$_3$] complex not previously reported, namely tris(trifluoroacetylacetonato)-manganese(III), [Mn(tfaa)$_3$] (Figure 1), is presented here and compared to previously published related structures. The crystal packing effects due to F···F non-covalent interactions are also reported. Experimental structural results obtained are complemented by a DFT study.

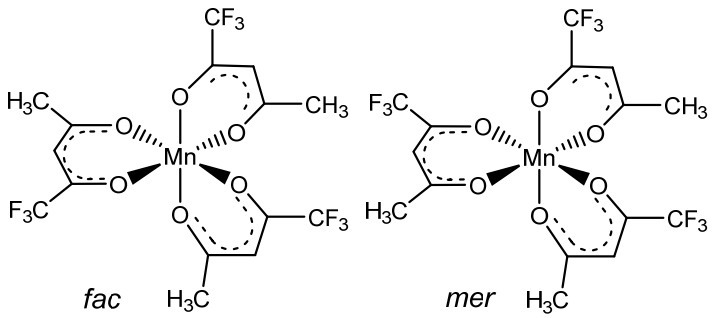

Figure 1. Structure of the two isomers possible for the tris(trifluoroacetylacetonato)-manganese(III), [Mn(tfaa)$_3$], complex of this study: *fac* and *mer*.

2 Results and discussion

2.1 Crystal structure

A diagram of the molecular structure of [Mn(tfaa)$_3$] is presented in **Figure 2**, while crystal data and structure refinement are summarised in **Table 1**. **Table 2** compares selected geometrical data of [Mn(tfaa)$_3$] with related [Mn(β-diketonato)$_3$] complexes, β-diketonato = (RCOCHCOR′)$^-$ with side groups R and R′ [21]. Additional crystallographic data is provided in the supplementary information. Two different molecules of [Mn(tfaa)$_3$], namely molecule A and molecule B, crystallized in the same asymmetric unit. [Mn(tfaa)$_3$] crystallized in the orthorhombic space group *Pca2$_1$*, with eight molecules in the unit cell. Both molecules are meridional isomers (*mer*), since the $O_{\beta\text{-diketonato}}$ atoms nearest to the three CF_3 groups, occupy a plane passing through the manganese atom.

The Mn-O bond lengths of molecule A range from 1.966(5) to 2.006(4) Å, consistent with a distorted octahedron, i.e. molecule A does not exhibit Jahn–Teller distortion. The Mn-O bond lengths of molecule B, however, can be viewed as two short bonds (1.924(4) and 1.939(4) Å) and four long bonds (1.985(5), 2.012(5), 2.047(5) and 2.061(5) Å), with the difference between the two shortest and four longest bonds 0.09 Å, consistent with moderate compression Jahn–Teller distortion, see **Figure 3**. Compression Jahn–Teller distortion is not common for structures of [Mn(β-diketonato)$_3$] complexes, and has only been reported for tris(acetylacetonato)-manganese(III), [Mn(acac)$_3$] [12,13] and tris(2,2,6,6-Tetramethylheptane-3,5-dionato-O,O')-manganese(III) [4] (**Table 2**). Moreover, the compression Jahn–Teller distortion observed for β-[Mn(acac)$_3$] was suggested to be the consequence of undetermined crystal packing effects [16]. Since neither molecules A and B exhibited the expected tetragonal elongation Jahn-Teller distortion (TE), we decided to further explore the character and strength of the intermolecular interactions, which might play a role in the observed distorted octahedron (DO, molecule A) and tetragonal compression Jahn–Teller distortion (TC, molecule B), both experimentally (crystal packing section 2.2) as well as theoretically by DFT methods (section 2.3).

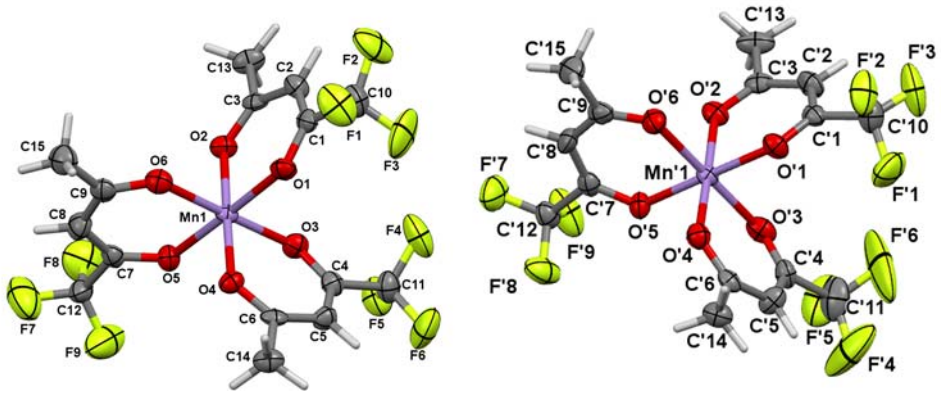

Figure 2: A perspective drawing of the molecular structure of molecule A (left) and molecule B (right) of [Mn(tfaa)$_3$], showing the atom numbering scheme. Atomic displacement parameters (ADPs) are shown at the 50 % probability level.

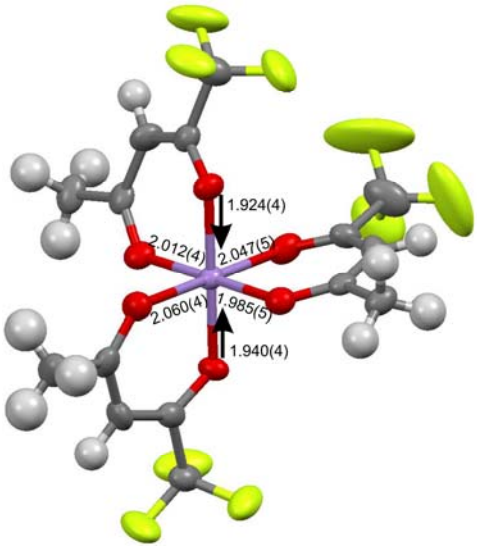

Figure 3: Molecule B of [Mn(tfaa)$_3$] showing Mn-O distances, showing moderate compression Jahn-Teller distortion.

Table 1: Crystal data and structure refinement of [Mn(tfaa)$_3$].

Empirical formula	C_{15} H_{12} F_9 Mn O_6
Formula weight	514.19
Temperature	150(2) K
Wavelength	0.71073 Å
Crystal system	Orthorhombic
Space group	$Pca2_1$
Unit cell dimensions	a = 14.6540(10) Å b = 19.8572(8) Å c = 13.3915(7) Å α= 90° β= 90° γ = 90°
Volume	3896.8(4) Å^3
Z	8
Density (calculated)	1.753 Mg/m^3
Absorption coefficient	0.792 mm^{-1}
F(000)	2048
Crystal size	0.400 x 0.200 x 0.200 mm^3
Theta range for data collection	2.301 to 25.113°.
Index ranges	-17<=h<=17, -23<=k<=23, -15<=l<=15
Reflections collected	128022
Independent reflections	6943 [R(int) = 0.0487]
Completeness to theta = 25.113°	99.9 %
Refinement method	Full-matrix least-squares on F^2
Data / restraints / parameters	6943 / 1 / 566
Goodness-of-fit on F^2	1.071
Final R indices [I>2sigma(I)]	R1 = 0.0543, wR2 = 0.1505
R indices (all data)	R1 = 0.0563, wR2 = 0.1527
Absolute structure parameter	0.10(3)
Extinction coefficient	n/a
Largest diff. peak and hole	1.428 and -0.531 e.Å^{-3}

Table 2: Selected geometric parameters for [Mn(III)(β-diketonato)$_3$] complexes, β-diketonato = (RCOCHCOR′)$^-$

β-diketonato	R	R′	Mn–O (Å) 1	2	3	4	5	6	Distortion	Distortion amount (Å)[a]	CSD ref code	Ref	Temp
acac[b]	CH_3	CH_3	1.931(10)	1.956(7)	1.984(8)	1.991(7)	2.003(8)	2.020(7)	moderate compression	0.05	ACACMN02	12	RT
			1.931(3)	1.933(3)	1.934(4)	1.942(3)	2.109(3)	2.112(4)	elongation	0.18	ACACMN21		RT
			1.895(8)	1.937(8)	2.004(11)	2.006(10)	2.034(9)	2.046(8)	not clear[c]	-	ACACMN23	11	293 K
			1.901(2)	1.930(2)	1.976(2)	1.984(2)	2.106(2)	2.111(2)	orthorhombic	-	ACACMN22	11	100 K
			1.914(2)	1.926(2)	1.981(2)	1.984(2)	2.082(2)	2.090(2)	orthorhombic	-	ACACMN22	11	100 K
			1.982	1.982	1.983	1.983	1.983	1.983	octahedral		VAGRAY	22	123 K
			1.940(3)	1.945(3)	1.957(3)	1.958(3)	2.060(3)	2.078(4)	slight elongation	0.12	XESPIW	23	RT
			1.924(1)	1.926(1)	1.929(1)	1.935(1)	2.127(1)	2.152(1)	elongation	0.21	ACACMN25	24	100 K
			1.898(2)	1.935(2)	1.965(2)	1.977(2)	2.102(2)	2.109(2)	elongation	0.16	ACACMN26	24	100 K
			1.932(5)	1.932(5)	1.946(5)	1.946(5)	2.157(16)	2.157(16)	elongation	0.22	[d]	17	398 K
dbm	Ph	Ph	1.89(2)	1.91(2)	1.92(2)	1.93(2)	2.09(2)	2.13(3)	elongation	0.20	JINPIF	15	RT
			1.908(2)	1.917(2)	1.931(2)	1.935(2)	2.109(2)	2.142(2)	elongation	0.20	JINPIF01	9	RT
			1.904(1)	1.915(1)	1.920(1)	1.924(1)	2.122(1)	2.160(1)	elongation	0.23	JINPIF02	25	100 K
			1.905(1)	1.915(1)	1.921(1)	1.924(1)	2.122(1)	2.159(1)	elongation	0.22	JINPIF03	26	150 K
			1.902(3)	1.927(3)	1.930(3)	1.941(4)	2.116(3)	2.141(4)	elongation	0.20	NOSHUA	27	RT
dpm	CMe_3	CMe_3	1.901	1.901	2.028	2.028	2.036	2.036	compression	0.13	QAYYEU	4	153 K
fca	Fc	CH_3	1.979	1.984	1.991	1.994	2.014	2.018	elongation	0.02	QAJNUN	28	150 K
	Ph	CHF_2	1.978	1.978	1.978	1.995	1.995	1.995	distorted octahedron	-	FAHLAE	8	298 K
tfth	CF_3	C_4H_3S	1.908(3)	1.921(4)	1.923(4)	1.931(4)	2.096(4)	2.109(4)	elongation	0.18	ALIQOD	20	RT
tfth	CF_3	C_4H_3S	1.904(4)	1.912(3)	1.919(4)	1.920(3)	2.128(4)	2.141(4)	elongation	0.22	ALIQOD01	20	150 K
tfaa	CH_3	CF_3	1.966(5)	1.975(5)	1.978(5)	2.004(5)	2.004(5)	2.006(4)	distorted octahedron	-	molecule A	this study	150 K
tfaa	CH_3	CF_3	1.924(4)	1.939(4)	1.985(5)	2.012(5)	2.047(5)	2.061(5)	moderate compression	0.09	molecule B	this study	150 K

a The difference between the two longest and four shortest bonds for elongation, and between the two shortest and four longest bonds for compression Jahn–Teller distortion.
b Selected structures
c The standard deviation on inter atomic distances is too large.
d gas-phase electron diffraction (GED)

2.2 Crystal packing

The packing of the [Mn(tfaa)$_3$] molecules in the solid state, exhibits various intermolecular interactions. Table 3 lists selected intermolecular interactions. Three unique F···F non-covalent intermolecular interactions (F6···F'1, F3···F'7 and F8···F'3), as well as a couple of F···H intermolecular interactions, for which the intermolecular distance between the atoms involved is less than the sum of the van der Waals radii, contribute to the packing observed. The intermolecular distance of the F···F and F···H interactions is given in **Table 3** and illustrated in **Figure 4**, **Figure 5** and **Figure 6**. **Table 4** lists selected interatomic angles and dihedrals involved in the intermolecular interactions between two [Mn(tfaa)$_3$] molecules A and B of this study. The three observed F···F intermolecular interactions of significance clearly direct and stabilize the packing of the molecules in the solid state. All these F···F interactions occur exclusively only between molecule A and molecule B, the two independent molecules present in the asymmetric units. For the F6···F'1 interaction, the C11-F6-F'1 angle is 150.3(5)° and the C'10-F'1-F6 angle is equal to that value, within 3 esd's, at 149.0(5)°. For the interaction observed between F8 and F'3, the C12-F8-F'3 angle is 97.6(5)° and the C'10-F'3-F8 angle is 170.7(5)°, the first angle nearer to 90° and the latter nearer to 180°. The latter two F···F interactions can be described as type-I and type-II halogen bonding [29], though F···F interactions are not always considered proper halogen bonds [30]. **Figure 4** depicts the molecular packing viewed along the c-direction. The packing clearly reflects the different channels formed by molecules A and B respectively, with the F···F and F···H (F3....H'8) interactions between the two molecules (A and B) present in the asymmetric unit. **Figure 6** compares the different lengths of the intermolecular interactions between molecules A in the one layer and molecules B in the other layer in the crystal to each other and to the sum of the van der Walls radii of the atoms involved. Intermolecular F···H interactions between different molecules A in the one channel (F9....H2) and between different molecules B in the next channel (F'8....H'2, F'2....H'1B, F'9....H'1H, F'2....H'1F and F'9....H'1C) stabilize the packing of the molecules in the channels of molecules (**Figure 4**).

The above described intermolecular F···F and F···H interactions in the experimental solid state crystal can distort the coordination polyhedron of the [Mn(tfaa)$_3$] crystal of this study, from the expected ^{5}B electronic state with elongation Jahn-Teller, to the observed higher energy ^{5}A electronic state with compression Jahn-Teller distortion (TE, molecule B) as well as the distorted octahedron (DO, molecule A).

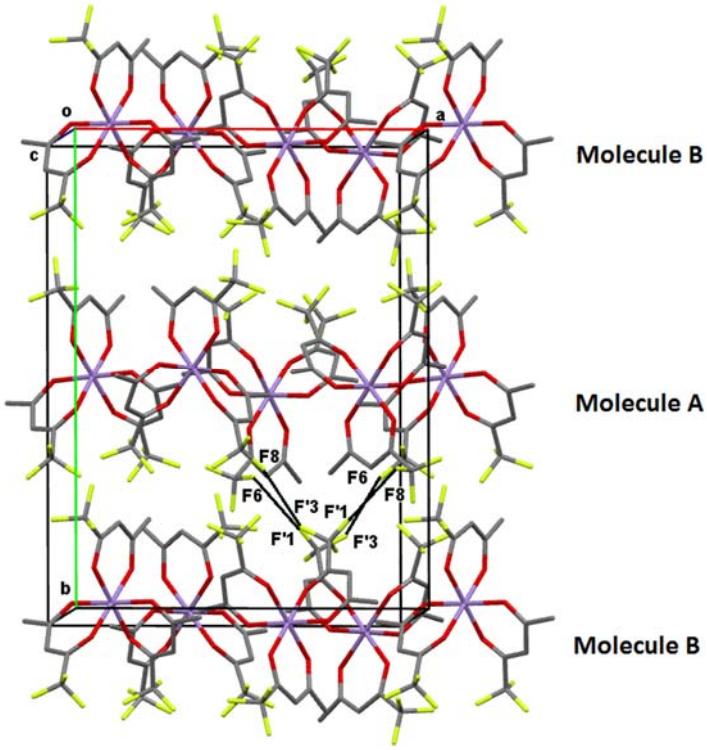

Figure 4. Crystal packing viewed along the c-direction, showing the Type I and Type II F···F interactions, F8···F'3 and F6···F'1 respectively.

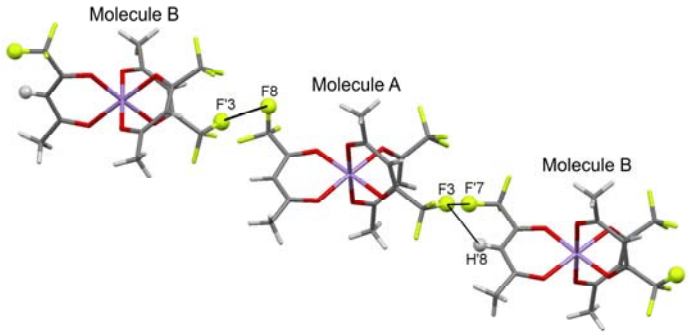

Figure 5. Crystal packing indicating the F3....H'8, F8....F'3 and F3....F'7 interactions viewed along the a-axis.

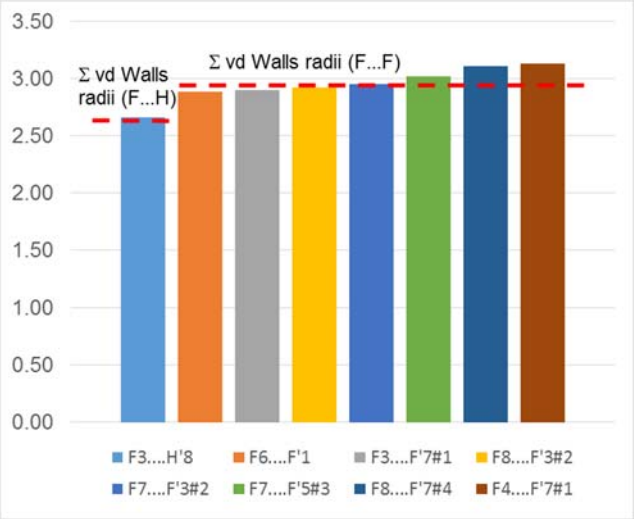

Figure 6. Visualization of the lengths (y-axis in Å) of the intermolecular F···H and F···F interactions between molecules A and molecules B, in different layers in the crystal.

Table 3. Selected distances related to intermolecular interactions between atom I and atom J, for the [Mn(tfaa)$_3$] crystal of this study.

I...J	**d(I-J) / Å**		**Sum van der Waals radii / Å**
Intermolecular (Molecule A)			
F9....H2	2.4	<<	2.67
Intermolecular (Molecule B)			
F'8....H'2	2.43	<<	2.67
F'2....H'1B	2.62	<	2.67
F'9....H'1H	2.63	<	2.67
F'2....H'1F	2.64	<	2.67
F'9....H'1C	2.66	<	2.67
Intermolecular			
F3....H'8	2.66	<	2.67
F'1....F6	2.882(8)	<	2.94
F'7....F3	2.898(9)	<	2.94
F'3....F8	2.923(9)	<	2.94
F'3....F7	2.949(10)		2.94
F'5....F7	3.016(10)		2.94
F'7....F8	3.110(8)		2.94
F'7....F4	3.133(8)		2.94

Symmetry transformations used to generate equivalent atoms:

#1 -x+1,-y+2,z+1/2 #2 x-1/2,-y+1,z #3 -x+1,-y+1,z+1/2 #4 x,y-1,z

Table 4. Selected interatomic C---F---F angles (deg) and C---F---F---C dihedral angles (deg), related to intermolecular interactions between two [Mn(tfaa)$_3$] molecules A and B of this study.

angle	
C10-F3-F'7#1	146.5(6)
C'12#1-F7#-F3	123.0(5)
C11-F4-F'7#1	94.2(4)
C'12#1-F'7#1-F4	110.7(5)
C11F6-F'1	150.3(5)
C'10-F'1 -F6	149.0(5)
C12-F7-F'3#2	97.1(5)
C'10#2- F'3#2-F7	130.1(6)
C12-F7-F'5#3	146.6(6)
C'11#3- F'5#3-F7	128.2(6)
C12-F8-F'3#2	97.6(5)
C'10#2- F'3#2-F8	170.7(5)
C12-F8-F'7#4	113.4(5)
C'12#4- F'7#4-F8	98.6(5)
dihedral	
C10-F3-F'7#1-C'12#1	-162.4(10)
C11-F4-F'7#1-C'12#1	110.1(6)
C11-F6-F'1-C'10	-130.8(14)
C12-F7-F'3#2-C'10#2	-148.3(8)
C12-F7-F'5#3-C'11#3	18.8(14)
C12-F8-F'3#2-C'10#2	12(4)
C12-F8-F'7#4-C'12#4	92.8(7)

Symmetry transformations used to generate equivalent atoms:

#1 -x+1,-y+2,z+1/2 #2 x-1/2,-y+1,z #3 -x+1,-y+1,z+1/2 #4 x,y-1,z

2.3 DFT study

The arrangement of the three trifluoroacetylacetonato ligands around Mn, leads to either a *fac* or a *mer* isomer (**Figure 1**). The DFT optimized geometry of the *mer* isomer was found to be slightly lower in energy, by *c.a*. 1 kcal/mol (0.04 eV), than the *fac* isomer [31]. The lower energy *mer* isomer was isolated in the solid state in this study. Optimizing molecule A and molecule B, using the coordinates of the crystal structures of A and B as input respectively, led both to molecules with elongation Jahn-Teller, though along different bonds, see **Figure 7**. The distorted octahedron geometry of molecule A (**Figure 7** a) optimized to a tetragonal elongation along opposite CF_3 – CF_3 bonds of (**Figure 7** b). The tetragonal compressed geometry of molecule B (**Figure 7** c) optimized to a tetragonal elongation along opposite CF_3 – CH_3 bonds of (**Figure 7** d). The calculated dipole moment of molecule A (DO) and optimized molecule A (TE along opposite CF_3 – CF_3 bonds) is 3.1 - 3.4 Debye, pointing slightly off-centre between two adjacent CF_3 groups. The calculated dipole moment of B (TC) and optimized molecule B (TE along opposite CF_3 – CH_3 bonds) is ca 4.2 Debye, pointing slightly off-centre between two adjacent CH_3 groups instead. The calculated dipole moment

an optimized TE molecule of [Mn(acac)$_3$] is 1.0 Debye, pointing exactly between two adjacent CH_3 groups, perpendicular to the direction of the elongated axis.

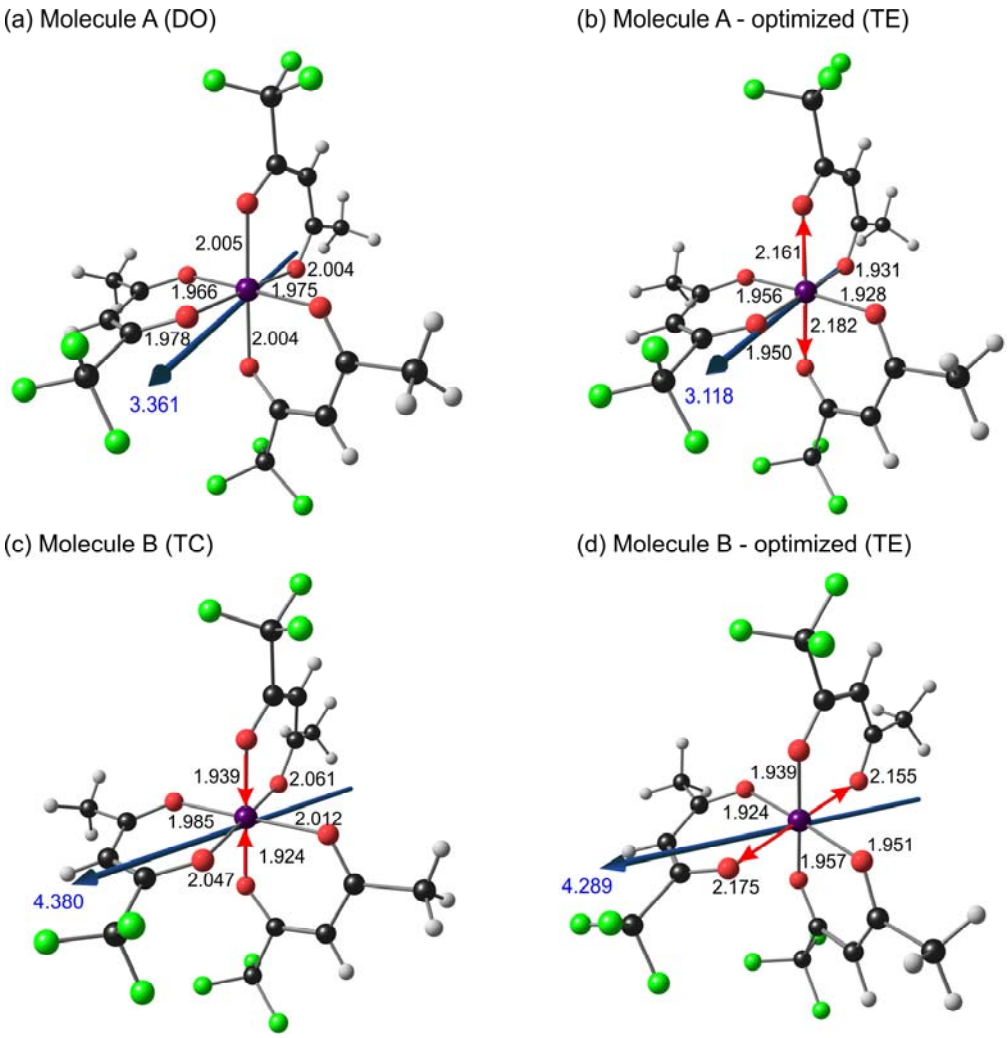

Figure 7: B3LYP/TZP single point and optimized structures of molecules A and B of [Mn(tfaa)$_3$] molecules, showing Mn-O bond lengths (black, angstrom) and the calculated dipole moment (blue arrow, value in Debye).

We further present here a Quantum Theory of Atoms in Molecules (QTAIM) study on selected molecular pairs, showing F···F interactions to illustrate that the experimentally observed intermolecular interactions are also identified as bond paths (BP) between atoms (atom critical points ACP), with bond critical points (BCP). According to the QTAIM theory, the existence of a bond path between a donor atom and an acceptor atom, as well as a bond critical point (BCP) between them, are sufficient criteria to establish bond existence [32]. The QTAIM theory provides topological descriptors, such as the electron density (ρ / e a_0^{-3}) and the Laplacian of electron density ($\nabla^2\rho$ / e a_0^{-5})

at the BCP, which have been used to characterize the strength of hydrogen bonds in various molecular systems. The descriptors (ρ and $\nabla^2\rho$) can also be used to distinguish between covalent and ionic bonding, hydrogen bonding, and van der Waals (vdW) interactions [33]. A negative Laplacian of electron density ($\nabla^2\rho$ / e a_0^{-5}) indicates a concentration of electron density. For BCP, negative $\nabla^2\rho$ is indicative of a covalent bonding, while positive $\nabla^2\rho$ indicates non-covalent bonding [34]. A small value of the electron density (ρ / e a_0^{-3}) and a positive value of its Laplacian are indicative of closed shell interactions, such as weak hydrogen bonds and van der Waals interactions. For example, for H-bonded complexes, $\rho \sim 10^{-2}$ a.u. or less, and for van der Waals complexes, $\rho \sim 10^{-3}$ a.u. with $\nabla^2\rho > 0$ [35]. Generally, larger electron density values for BCP indicate stronger interactions [36,37]. Furthermore, since the electron density at hydrogen bond critical points increases approximately linearly with increasing stabilization energy in going from weak hydrogen bonds to moderate and strong hydrogen bonds, it can be used as an indicator of the nature and gradual change of strength of the hydrogen bond [33].

To illustrate that the experimentally identified short F···F intermolecular contacts can also be described in terms of electron density distribution between atoms according to the QTAIM theory, three pairs of [Mn(tfaa)$_3$] molecules, which showed the F8···F'3 (molecular pair 1), F6···F'1 (molecular pair 2), and F3···F'7 (molecular pair 3) interactions respectively, have been selected from the crystal data. B3LYP-D3/TZP single point calculations, including a QTAIM analysis, have been done on each of the three molecular pairs separately, in order to determine the intermolecular bond paths between the molecular pairs. **Figure 8** illustrates the results obtained from the QTAIM analysis of the three molecular pairs, showing the intra- and intermolecular bond paths obtained. **Table 5** gives a summary of the topological parameters of selected bond critical points. All three molecular pairs (**Figure 8** and **Table 5**) exhibit 86 atom critical points (ACP) and at least 6 ring critical points (RCP), since each molecule has 43 atoms and three pseudo aromatic trifluoroacetylacetonato ring systems. Additional BCP's and RCP's identified for the molecular pairs, are due to intra- and intermolecular bonds. The electron density (ρ) and its Laplacian ($\nabla^2\rho$) of the additional BCP's are both positive, indicative of weak non-covalent hydrogen and of fluorine-centered non-covalent bonding interactions [38].

In molecular pair 1 (**Figure 8**a) one intra- (F'6···F'1) and three intermolecular BCP (F8···F'3, F7···F'3, H8···F'3) were obtained. The intermolecular BCP all involve F'3, with the two non-covalent F···F bonds (F8···F'3, F7···F'3) stronger than the weak F···H hydrogen bond (H8···F'3). The same three

intermolecular interactions were experimentally observed for molecular pair 1 (Table 3, **Figure 4**, **Figure 8**a). The two additional RCP's (125 and 129 in **Figure 8**a) obtained by the QTAIM analysis for molecular pair 1, are both related to the rings formed by the three intermolecular BCP's involving F'3. The ρ and its $\nabla^2\rho$ of RCP125 and RCP129 are much lower than that of the six RCP's of the pseudo aromatic trifluoroacetylacetonato ring systems formed by covalent bonds, consistent with the weaker intermolecular bonds involved in the rings round RCP125 and RCP129. In molecular pair 2 (**Figure 8**b) one intra- (F'6···F'1, the same as obtained in molecular pair 1) and one intermolecular BCP (F6....F'1) were obtained, both non-covalent F···F bonds involving F'1, in agreement with experimental observation (Table 3, **Figure 4**, **Figure 8**b). In molecular pair 3 (**Figure 8**c) one intra- (F'6···F'1, the same as obtained in molecular pair 1 and 2) and five intermolecular BCP (F3···F'7, F4···F'7, F6···F'7, C5···F'7, F3···H'8) were obtained. The F···F' intermolecular BCP's all involve F'7, of which F3···F'7 is the strongest. The F3···F'7, F4···F'7, F6···F'7 and F3···H'8 intermolecular interactions were also experimentally observed (Table 3, **Figure 4**, **Figure 8**c). The three additional RCP's (103, 144 and 157 in **Figure 8**c) obtained by the QTAIM analysis for molecular pair 3, are related to the rings formed by the three inter- molecular BCP's involving F'7. Similar to that of molecular pair 1, the ρ and its $\nabla^2\rho$ of RCP103, RCP144 and RCP157 are much lower than that of the six RCP's of the pseudo aromatic trifluoroacetylacetonato ring systems formed by covalent bonds, consistent with the weaker intermolecular bonds involved in the rings round RCP103, RCP144 and RCP157.

The obtained values of ρ (*c.a.* 0.0051) and its $\nabla^2\rho$ (0.027 – 0.029) of the BCP related to the strongest intermolecular BCP involving fluorines, F8···F'3 and F7···F'3 (molecular pair 1), F6···F'1 (molecular pair 2), and F3···F'7 (molecular pair 3), fall well into the range proposed for ρ and its $\nabla^2\rho$ for a hydrogen bond to exist, namely 0.002-0.035 e a_0^{-3} and 0.016-0.139 e a_0^{-5} [39]. Intermolecular bond with ρ of *c.a.* 0.004 – 0.02 e a_0^{-3} is considered weak (van der Waals) hydrogen bonds [33]. The values of ρ (*c.a.* 0.0051) obtained for the F···F inter- molecular interaction in this study, is slightly higher than the reported ρ values for F···F interactions in a number of molecules optimized at the RI-MP2/def2-TZVPD level of theory, that range from 0.0027 – 0.0036 [40]. It can thus be concluded that the QTAIM study agrees with experimental observation in that the different $[Mn(tfaa)_3]$ molecules are connected by weak intermolecular halogen bonds.

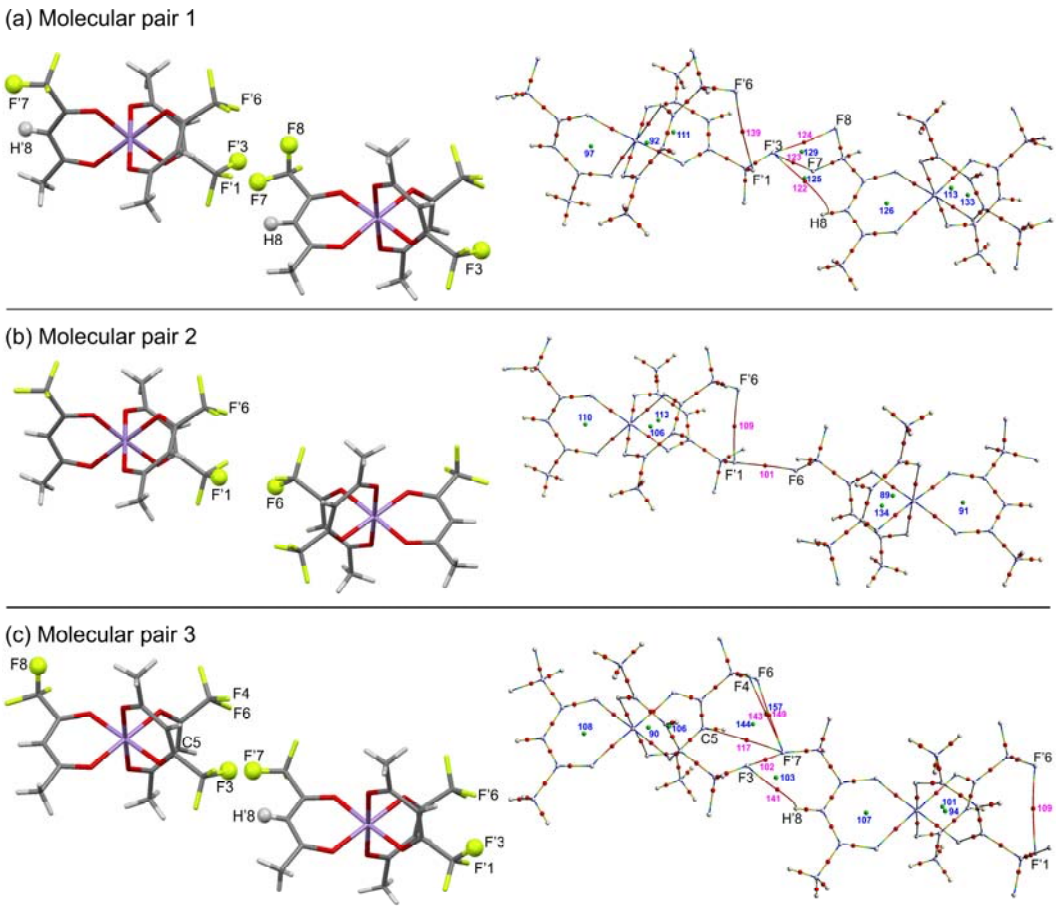

Figure 8: QTAIM determined intermolecular bond-paths (BP), bond critical points (BCP in red) and ring critical points (RCP in green) between three pairs of [Mn(tfaa)$_3$] molecules. Selected atom numbers, according to the numbering scheme in **Figure 2**, are shown in black font. The numbers of selected intra- and intermolecular bond paths (magenta) and ring critical points (blue) are also shown. Left are the three molecular pairs from the crystal and right, QTAIM results on the same three molecular pairs. The colour of the bond-paths changes according to electron density, from blue (high density) to green to red (low density).

Table 5: Topological parameters of the QTAIM calculated intermolecular bonds between three [Mn(tfaa)$_3$] pairs. The numbers of selected critical points (CP) are shown in Figure 8.

	Bond path (BP) number	Atom1 involved	Atom 2 involved	Inter-atomic distance / Å	BP length / Å	Electron density ρ / e a_0^{-3}	Laplacian of electron density $\nabla^2\rho$ / e a_0^{-5}
Molecular pair 1	**(94 BCP, 8 RCP, 86 ACP)**						
intramolecular BCP	139[a]	F'6	F'1	3.3927	3.3993	0.0018	0.0086
intermolecular BCP	122	H8	F'3	3.082	3.4388	0.0029	0.0117
	123	F7	F'3	2.9487	2.9518	0.0051	0.0273
	124	F8	F'3	2.923	2.927	0.0048	0.0274
ring critical point (RCP)	92					0.0147	0.0821
	97					0.0152	0.0843
	111					0.0160	0.0907
	113					0.0155	0.0868

	125					0.0027	0.0120
	126					0.0151	0.0854
	129					0.0042	0.0236
	133					0.0157	0.0887
Molecular pair 2	**(92 BCP, 6 RCP, 86 ACP)**						
intramolecular BCP	109 [a]	F'1	F'6	3.3927	3.3993	0.0018	0.0086
intermolecular BCP	101	F'1	F6	2.8817	2.888	0.0045	0.0272
ring critical point (RCP)	89					0.1548	0.0868
	91					0.0151	0.0854
	106					0.0147	0.0822
	110					0.0152	0.0843
	113					0.0160	0.0907
	134					0.0157	0.0887
Molecular pair 3	**(96 BCP, 9 RCP, 86 ACP)**						
intramolecular BCP	109 [a]	F'6	F'1	3.3927	3.3994	0.0018	0.0086
intermolecular BCP	102	F3	F'7	2.8981	2.9034	0.0051	0.0287
	117	C5	F'7	3.4663	3.5239	0.0029	0.0116
	141	F3	H'8	2.6616	2.713	0.0045	0.0211
	143	F4	F'7	3.1328	3.1355	0.0037	0.0180
	149	F6	F'7	3.2336	3.2368	0.0030	0.0149
ring critical point (RCP)	90					0.0155	0.0869
	94					0.0160	0.0908
	101					0.0147	0.0821
	103					0.0034	0.0167
	106					0.0157	0.0887
	107					0.0152	0.0843
	108					0.0151	0.0853
	144					0.0023	0.0106
	157					0.0029	0.0147

a The intramolecular BCP refers to the same atoms (F'6 and F'1) in molecular pair 1, 2 and 3

3 Experimental Section

3.1 Synthesis

The $[Mn(tfaa)_3]$ complex was synthesized by a procedure adapted from literature [41] according to a published method [42]. $[Mn(tfaa)_3]$ is a high spin paramagnetic complex [10].

Characterization data for tris(trifluoroacetylacetonato)-manganese(III), $[Mn(tfaa)_3]$

Yield 69 %. Colour: Dark brown-black. Melting point 116.7 °C. MS The calculated value for $MnC_{15}H_{12}O_6F_9$ = 514.18 g/mol, Found: 514.50 g/mol. Elemental analysis; Calculated for $MnC_{15}H_{12}O_6F_9$: C, 35.0; H, 2.4 Found: C, 33.6; H, 2.3.

3.2 Crystal structure analysis

Data for tris(trifluoroacetylacetonato)-manganese(III), [Mn(tfaa)$_3$] was collected at 150 K on a Bruker D8 Venture kappa geometry diffractometer, with duo Iμs sources, a Photon 100 CMOS detector and APEX II [43] control software, using Quazar multi-layer optics, monochromated Mo-*K*α radiation, by means of a combination of ϕ and ω scans. Data reduction was performed using SAINT+ [43] and the intensities were corrected for absorption, using SADABS [43]. The structure was solved by intrinsic phasing, using SHELXTS, and refined by full-matrix least squares, using both SHELXTL+ [44] and SHELXL-2017+ [44]. In the structure refinement, all hydrogen atoms were added in the calculated positions and treated as riding on the atom to which they are attached. All non-hydrogen atoms were refined with anisotropic displacement parameters; all isotropic displacement parameters for hydrogen atoms were calculated as ($X \times U_{eq}$) of the atom to which they are attached, where X = 1.2 for all hydrogen atoms. Crystal data, data collection, structure solution and refinement details are available in the CIF (CCDC deposit number 1828317).

3.3 DFT calculations

Density functional theory (DFT) calculations were conducted with the Amsterdam Density Functional (ADF 2016 and updates) programme [45,46,47] with hybrid functional B3LYP [48,49] (20% Hartree-Fock exchange) in combination with the Grimme empirical dispersion correction D3 [50], with an all-electron TZP (Triple ζ polarised) basis set, while spin-unrestricted open shell calculations were used for geometry optimisation. The B3LYP functional proved to correctly calculate the high spin (S = 2) ground state of [Mn(β-diketonato)$_3$] [20,25,31]. The analysis of the noncovalent interactions involved in the complexes were done with Bader's quantum theory of atoms in molecules (QTAIM) [51,52,53] as implemented in ADF.

4 Conclusions

Various intermolecular F···F and F···H interactions, with lengths shorter than the sum of the van der Waals radii of the atoms involved, are identified in the experimental solid state crystal of [Mn(tfaa)$_3$]. A Quantum Theory of Atoms in Molecules study on selected molecular pairs of [Mn(tfaa)$_3$], confirms the existence of the experimentally identified intermolecular halogen bonds with QTAIM calculated topological descriptors in agreement with criteria for hydrogen bonds and non-covalent intermolecular F···F interactions. The various intermolecular F···F and F···H interactions between the [Mn(tfaa)$_3$] molecules in the solid crystalline state, contribute to the distortion of the coordination polyhedron of [Mn(tfaa)$_3$] from the expected ^{5}B electronic state with elongation Jahn-Teller, to the

observed higher energy ^{5}A electronic state with compression Jahn-Teller distortion (molecule B) and the distorted octahedron (molecule A).

Acknowledgments

The authors acknowledge financial support from the South African National Research Foundation (Grant numbers 113327, 96111) and the Central Research Fund of the University of the Free State, Bloemfontein, South Africa. The CHPC of South Africa, the HPC of the UFS and the Norwegian Supercomputing Program (UNINETT Sigma2, Grant No. NN9684K) are acknowledged for computer time.

References

[1] Y.-F. Wang, S. Chiba, Mn(III)-Mediated Reactions of Cyclopropanols with Vinyl Azides: Synthesis of Pyridine and 2-Azabicyclo[3.3.1]non-2-en-1-ol Derivatives, J. Am. Chem. Soc. 131 (2009) 12570-12572. DOI:10.1021/ja905110c

[2] M.J.S. Dewar, T. Nakaya, Oxidative coupling of phenols, J. Am. Chem. Soc. 90 (1968) 7134-7135. DOI:10.1021/ja01027a051

[3] R.I. Khusnutdinov, N.A. Shchadneva, A.R. Baiguzina, Yu.Yu. Lavrentieva, U.M. Dzhemilev, Generation of alkyl hypochlorites in oxidation of alcohols with carbon tetrachloride catalyzed by vanadium and manganese compounds, Russ. Chem. Bull. Int. Ed. 51 (2002) 2074-2079. DOI:10.1023/A:1021668011691

[4] P. Magnus, A.H. Payne, M.J. Waring, D.A. Scott, V. Lynch, Conversion of α,β-unsaturated ketones into α-hydroxy ketones using an MnIII catalyst, phenylsilane and dioxygen: acceleration of conjugate hydride reduction by dioxygen, Tetrahedron Lett. 41 (2000) 9725–9730. . (CCDC 158103, reference QAYYEU) DOI:10.1016/S0040-4039(00)01727-5

[5] J.R. Bryant, J.E. Taves, J.M. Mayer, Oxidations of Hydrocarbons by Manganese(III) Tris(hexafluoroacetylacetonate), Inorg. Chem. 41 (2002) 2769-2776. DOI:10.1021/ic025541z

[6] R. van Gorkum, E. Bouwman, J. Reedijk, Fast Autoxidation of Ethyl Linoleate Catalyzed by [Mn(acac)$_3$] and Bipyridine: A Possible Drying Catalyst for Alkyd Paints, Inorg. Chem. 43 (2004) 2456-2458. DOI:10.1021/ic0354217

[7] R.K. Sodhi, S. Paul, Nanosized Mn(acac)$_3$ Anchored on Amino Functionalized Silica for the Selective Oxidative Synthesis of 2-arylbenzimidazoles, 2-arylbenzothiazoles and Aerobic Oxidation of Benzoins in Water, Catal. Lett. 141 (2011) 608–615. DOI:10.1007/s10562-010-0540-8

[8] S. Carli, E. Benazzi, L. Casarin, T. Bernardi, V. Bertolasi, R. Argazzi, S. Caramoria, C.A. Bignozzi, On the stability of manganese tris(β-diketonate) complexes as redox mediators in DSSCs, Phys. Chem. Chem. Phys. 18 (2016) 5949-5956. DOI:10.1039/C5CP05524E

[9] A.L. Barra, D. Gatteschi, R. Sessoli, G.L. Abbati, A. Cornia, A.C. Fabretti, M.G. Uytterhoeven, Electronic Structure of Manganese(III) Compounds from High-Frequency EPR Spectra, Angew. Chem. Int. Ed. 36 (1997) 2329-2331. (CCDC 406981, reference JINPIF01) DOI:10.1002/anie.199723291

[10] S.L. Dexheimer, J.W. Gohdes, M.K. Chan, K.S. Hagen, W.H. Armstrong, M.P. Klein, Detection of EPR Spectra in S = 2 States of Trivalent Manganese Complexes, J. Am. Chem. Soc. 111 (1989) 8923-8925. DOI:10.1021/ja00206a028
[11] S. Geremia, N. Demitri, Crystallographic Study of Manganese(III) Acetylacetonate: An Advanced Undergraduate Project with Unexpected Challenges, J. Chem. Educ. 82 (2005) 460-465. DOI:10.1021/ed082p460
[12] J.P. Fackler, A. Avdeef, Crystal and molecular structure of tris(2,4-pentanedionato) manganese(III), $Mn(O_2C_5H_7)_3$, a distorted complex as predicted by Jahn-Teller arguments, Inorg. Chem. 13 (1974) 1864–1875. DOI:10.1021/ic50138a016
[13] R. Frohlich, R. Milan, S. Yadava, CCDC 692561, reference ACACMN24, Private communication (2008).
[14] B.R. Stults, R.S. Marianelli, V.W. Day, Distortions of the coordination polyhedron in high-spin manganese(III) complexes. 3. Crystal and molecular structure of gamma-tris(acetylacetonato)manganese(III): a tetragonally elongated octahedral form, Inorg. Chem. 18 (1979) 1853–1858. DOI:10.1021/ic50197a028
[15] E.G. Zaitseva, I.A. Baidina, P.A. Stabnikov, S.V. Borisov, I.K. Igumenov, Crystal and molecular structure of tris(dibenzoylmethanato)manganese(III), Zh. Strukt. Khim. (Russ.) (Russian Journal of Structural Chemistry) 31 (1990) 184-189. (CCDC reference JINPIF) DOI:10.1007/BF00752705
[16] J. Krzystek, G. Yeagle, J-H. Park, R.D. Britt, M.W. Meisel, L-C. Brunel, J. Telser, High-Frequency and -Field EPR Spectroscopy of Tris(2,4-pentanedionato)manganese(III): Investigation of Solid-State *versus* Solution Jahn-Teller Effects, Inorg. Chem. 42 (2003) 4610-4618. DOI:10.1021/ic020712l
[17] R.J.F. Berger, G.V. Girichev, N.I. Giricheva, A.A. Petrova, N.V. Tverdova, The Structure of $Mn(acac)_3$-Experimental Evidence of a Static Jahn–Teller Effect in the Gas Phase, Angew. Chem. Int. Ed. 56 (2017) 15751–15754. DOI:10.1002/anie.201708498
[18] R.J.F. Berger, G.V. Girichev, N.I. Giricheva, A.A. Petrova, V.V. Sliznev, N.V. Tverdova, Molecular structure of manganese tris-acetylacetonate in different spin states, Izv. Vyssh. Uchebn. Zaved. Khim. Khim. Tekhnol. 60 (2017) 47– 53. DOI:10.6060/tcct.2017604.5555
[19] J. Conradie, Bond stretch isomers of d tris(benzoylacetonato-κ^2O,O')Mn(III), Comput. Theor. Chem. 1087 (2016) 1-5. DOI:10.1016/j.comptc.2016.04.022
[20] R. Gostynski, P.H. van Rooyen, J. Conradie, Jahn-Teller Distortion in Tris[4,4,4-Trifluoro-1-(2-thienyl)-1,3-butanedionato]manganese(III) Isomers: an X-ray and Computational Study, J. Mol. Struct. 1119 (2016) 48-53. DOI:10.1016/j.molstruc.2016.04.048, http://www.journals.elsevier.com/journal-of-molecular-structure/
[21] Cambridge Structural Database (CSD), Version 5.38, May 2017 update, Cambridge, UK, 2017.
[22] N.F. Chilton, S.K. Langley, B. Moubaraki, K.S. Murray, Synthesis, structural and magnetic studies of an isostructural family of mixed 3d/4f tetranuclear 'star' clusters, Chem. Commun. 46 (2010) 7787–7789. DOI:10.1039/C0CC02642E
[23] Y. Cheng, S. Xia, J. Feng, S. Du, L. An, X. Lu, Solvothermal Synthesis and Crystal Structures of Two Manganese Complexes [Mn(II)(acac−)2(4,4′-bipy)]n (bipy=4,4′-bipyridine) and [Mn(III)(acac─)3]•4CO(NH2)2, Chin. J. Chem. 30 (2012) 1063-1068. DOI:10.1002/cjoc.201100520
[24] E. Arslan, R.A. Lalancette, I. Bernal, An historic and scientific study of the properties of metal(III) tris-acetylacetonates, Struct. Chem. 28 (2017) 201–212. DOI:10.1007/s11224-016-0864-0
[25] R. Freitag, T.J. Muller, J. Conradie, X-ray diffraction and DFT calculation elucidation of the Jahn-Teller effect observed in $Mn(dibenzoylmethanato)_3$, J. Chem. Cryst. 44 (2014) 352-359. DOI:10.1007/s10870-014-0522-6
[26] A. Prescimone, E. Brechin, CSD Communication (Private Communication), 2015, CCDC 1411114 reference JINPIF03.
[27] L. Chen, J. Wang, Y-Z. Liu, Y. Song, X-T. Chen, Y-Q. Zhang, Z-L. Xue, Slow Magnetic Relaxation in Mononuclear Octahedral Manganese(III) Complexes with Dibenzoylmethanide Ligands, Eur. J. Inorg. Chem. 2 (2015) 271-278. DOI:10.1002/ejic.201402964

[28] B.E. Buitendach, E. Erasmus, M. Landman, J.W.(Hans) Niemantsverdriet, J.C. Swarts, Consequences of Electron-Density Manipulations on the X-ray Photoelectron Spectroscopic Properties of Ferrocenyl-β-diketonato Complexes of Manganese(III). Structure of [$Mn(FcCOCHCOCH_3)_3$], Inorg. Chem. 55 (2016) 1992–2000. DOI:10.1021/acs.inorgchem.5b02250
[29] P.R. Varadwaj, A. Varadwaj, H.M. Marques, Halogen Bonding: A Halogen-Centered Noncovalent Interaction Yet to Be Understood, Inorganics 7 (2019) 40. DOI:10.3390/inorganics7030040
[30] A. Varadwaj, P.R. Varadwaj, K. Yamashita, Do Surfaces of Positive Electrostatic Potential on Different Halogen Derivatives in Molecules Attract? Like Attracting Like!, Journal of Computational Chemistry 39 (2018) 343–350. DOI:10.1002/jcc.25125
[31] R. Gostynski, J. Conradie, E. Erasmus, Significance of electron-density of molecular fragments on the properties of manganese(III) β-diketonato complexes: An XPS and DFT study, RSC Adv. 7 (2017) 27718-27728. DOI:10.1039/c7ra04921h
[32] R.F.W. Bader, A Bond Path: A Universal Indicator of Bonded Interactions, J. Phys. Chem. A 102 (1998) 7314–7323. DOI:10.1021/jp981794v
[33] R. Parthasarathi, V. Subramanian, N. Sathyamurthy, Hydrogen bonding without borders: An atoms-in-molecules perspective. J. Phys. Chem. A 110 (2006) 3349–3351. DOI:10.1021/jp060571z
[34] J. Platts, J. Overgaard, C. Jones, B.B. Iversen, A. Stasch, First experimental characterization of a non-nuclear attractor in a dimeric magnesium(I) compound, J. Phys. Chem. A 115 (2011) 194–200. DOI:10.1021/jp109547w
[35] P.S.V. Kumar, V. Raghavendra, V. Subramanian, Bader's Theory of Atoms in Molecules (AIM) and its Applications to Chemical Bonding, J. Chem. Sci. 128 (2016) 1527–1536. DOI:10.1007/s12039-016-1172-3
[36] I. Alkorta, F. Blanco, J. Elguero, J. Dobado, S.M. Ferrer, I. Vidal, Carbon-carbon weak interactions, J. Phys. Chem. A 113 (2009) 8387–8393. DOI:10.1021/jp903016e
[37] R.G.A. Bone, R.F.W. Bader, Identifying and Analyzing Intermolecular Bonding Interactions in van der Waals Molecules, J. Phys. Chem. 100 (1996) 10892–10911. DOI:10.1021/jp953512m
[38] A. Varadwaj, H.M. Marques, P.R. Varadwaj, Is the Fluorine in Molecules Dispersive? Is Molecular Electrostatic Potential a Valid Property to Explore Fluorine-Centered Non-Covalent Interactions?, Molecules 24 (2019) 379. DOI:10.3390/molecules24030379
[39] (a) M.T. Caroll, R.F.W. Bader, An analysis of the hydrogen bond in BASE-HF complexes using the theory of atoms in molecules, Mol. Phys. 65 (1988) 695-722. DOI:10.1080/00268978800101351
(b) M.T. Caroll, C. Chang, R.F.W. Bader, Prediction of the structures of hydrogen-bonded complexes using the laplacian of the charge density, Mol. Phys. 63 (1988) 387-405. DOI:10.1080/00268978800100281
(c) R.F.W. Bader, H. Essén, The characterization of atomic interactions, J. Chem. Phys. 80 (1984) 1943-1960. DOI:10.1063/1.446956
(d) P.L.A. Popelier, R.F.W. Bader, The existence of an intramolecular C-H-O hydrogen bond in creatine and carbamoyl sarcosine, Chem. Phys. Lett. 189 (1992) 542-548. DOI:10.1016/0009-2614(92)85247-8
(e) U. Koch, P.L.A. Popelier, Characterization of C-H-O Hydrogen Bonds on the Basis of the Charge Density, J. Phys. Chem. 99 (1995) 9747–9754. DOI:10.1021/j100024a016
[40] A. Bauzá, A. Frontera, Electrostatically enhanced F···F interactions through hydrogen bonding, halogen bonding and metal coordination: an ab initio study, Phys. Chem. Chem. Phys. 18 (2016) 20381. DOI: 10.1039/c6cp03862j
[41] M.N. Bhattacharjee, M.K. Chaudhuri, D.T. Khathing, Direct Synthesis of Tris(acetylacetonato)manganese(III), J. Chem. Soc., Dalton Trans. (1982) 669-670. DOI:10.1039/DT9820000669
[42] R. Freitag, J. Conradie, Electrochemical and Computational Chemistry Study of Mn(β-diketonato)$_3$ complexes. Electrochim. Acta 158 (2015) 418–426. DOI:10.1016/j.electacta.2015.01.147, http://www.journals.elsevier.com/electrochimica-acta/
[43] APEX2 (including SAINT and SADABS), Bruker AXS Inc., Madison, WI, 2012.

[44] G.M. Sheldrick, A short history of SHELX, Acta Crystallogr., Sect. A: Found. Crystallogr. A64 (2008) 112-122. DOI:10.1107/S0108767307043930
[45] G. te Velde, F.M Bickelhaupt, E.J. Baerends, C. Fonseca Guerra, S.J.A. van Gisbergen, J.G. Snijders, T. Ziegler, Chemistry with ADF, J. Comput. Chem. 22 (2001) 931-967. DOI:10.1002/jcc.1056
[46] C.F. Guerra, J.G. Snijders, G. te Velde, E.J. Baerends, Towards an order-N DFT method, Theor. Chem. Acc. 99 (1998) 391-403. DOI:10.1007/s002140050353
[47] ADF2016, SCM, Theoretical Chemistry, Vrije Universiteit, Amsterdam, The Netherlands, 2016. http://www.scm.com
[48] A.D. Becke, Density-functional exchange-energy approximation with correct asymptotic behaviour, Phys. Rev. A: At. Mol. Opt. Phys. A38 (1988) 3098-3100. DOI: 10.1103/PhysRevA.38.3098
[49] C.T. Lee, W.T. Yang, R.G. Parr, Development of the Colle-Salvetti correlation-energy formula into a functional of the electron-density, Phys. Rev. B: Condens. Matter B37 (1988) 785-789. DOI: 10.1103/PhysRevB.37.785
[50] S. Grimme, J. Antony, S. Ehrlich, H. Krieg, A consistent and accurate ab initio parametrization of density functional dispersion correction (DFT-D) for the 94 elements H-Pu, J. Chem. Phys. 132 (2010) 154104-154104. DOI:10.1063/1.3382344
[51] R.F.W. Bader, A quantum theory of molecular structure and its applications, Chemical Reviews 91 (1991) 893-928. DOI:10.1021/cr00005a013
[52] F. Cortés-Guzmán, R.F.W. Bader, Complementarity of QTAIM and MO theory in the study of bonding in donor–acceptor complexes, Coordination Chemistry Reviews 249 (2005) 633-662. DOI:10.1016/j.ccr.2004.08.022
[53] J.I. Rodríguez, R.F.W. Bader, P.W. Ayers, C. Michel, A.W. Götz, C. Bo, A high performance grid-based algorithm for computing QTAIM properties, Chemical Physics Letters 472 (2009) 149-152. DOI:10.1016/j.cplett.2009.02.081